

# Simultaneous X-Ray and Gamma-Ray Observations of TeV Blazars: Testing Synchro-Compton Emission Models and Probing the Infrared Extragalactic Background

Paolo S. Coppi

Department of Astronomy, Yale University, P.O. Box 208101, New Haven, CT 06520-8101

Felix A. Aharonian

Max-Planck-Institut für Kernphysik, Postfach 103980, D-69029 Heidelberg, Germany

*to appear in ApJ Lett., vol. 521, L33*

## ABSTRACT

The last years have seen a revolution in ground-based  $\gamma$ -ray detectors. We can now detect the spectra of nearby TeV blazars like Mrk 421 and 501 out to  $\sim 20$  TeV, and during the strongest flares, we can now follow fluctuations in these spectra on timescales close to the shortest ones likely in these objects. We point out that this represents a unique opportunity. Using these and future detectors in combination with broadband X-ray satellites like SAX and RXTE, we will be able to simultaneously follow all significant X-ray/ $\gamma$ -ray variations in a blazar's emission. This will provide the most stringent test yet of the synchrotron-Compton emission model for these objects. In preparation for the data to come, we present sample SSC model calculations using a fully self-consistent, accurate code to illustrate the variability behavior one might see and to show how good timing information can probe physical conditions in the source. If the model works, i.e., if X-ray/TeV variations are consistent with being produced by a common electron distribution, then we show it is possible to robustly estimate the blazar's intrinsic TeV spectrum from its X-ray spectrum. Knowing this spectrum, we can then determine the level of absorption in the observed spectrum. Constraining this absorption, due to  $\gamma$ -ray pair production on diffuse radiation, provides an important constraint on the infrared extragalactic background intensity. Without the intrinsic spectrum, we show that detecting absorption is very difficult and argue that Mrk 421 and 501, as close as they are, may already be absorbed by a factor 2 at  $\sim 3$  TeV. This should not be ignored when fitting emission models to the spectra of these objects.

*Subject headings:* cosmology: diffuse radiation — gamma rays: theory — galaxies: active

## 1. Introduction

Recent broadband spectral compilations (e.g., see Ulrich, Maraschi, & Urry 1997) suggest that blazars can be divided into two rough classes, “LBL” and “HBL,” depending on the energy where their synchrotron emission peaks (optical/UV for LBL, and UV/X-ray for HBL). As expected in a synchrotron-Compton (SC) jet emission model where the synchrotron-emitting electrons also Compton upscatter photons to  $\gamma$ -ray energies (see, e.g., Sikora 1997 and Coppi 1997 for reviews of current blazar emission models and controversies), the energy of their  $\gamma$ -ray emission peak (MeV/GeV in LBLs, GeV/TeV in HBLs) is well-correlated with that of the synchrotron peak. Most work to date has focused on LBL objects like 3C 279, probably because these objects are the ones associated with the most powerful, classical radio sources and also simply because they were the only ones accessible in the  $\gamma$ -ray domain (via EGRET observations). In this Letter, we argue that equal if not more effort should now be devoted to the weak and “uninteresting” nearby HBLs like Mrk 421 and 501; the scientific payoff is potentially much larger. The new development is the arrival of powerful, ground-based Cherenkov telescope arrays (e.g., see Aharonian & Akerlof 1997). Such detectors have enormous collection areas (up to  $10^9$  cm<sup>2</sup> vs. 1500 cm<sup>2</sup> for EGRET), and the already existing HEGRA array can follow  $\sim 500$  GeV- 10 TeV spectral variations in Mrk 421/501 down to  $\sim$  one hour timescales (e.g., see Aharonian et al. 1999a). The sensitivity and energy coverage will significantly improve once new and larger arrays like VERITAS and HESS come online. This range of timescales and spectral coverage is well-matched to the capabilities of modern broadband X-ray detectors like ASCA, RXTE, and SAX that can monitor fluctuations in the synchrotron emission between  $\sim 1$ -200 keV. Using HBLs, for the first time we can thus hope to follow and resolve simultaneously *all* significant fluctuations in the putative synchrotron and Compton emission components of a blazar.

This has two important consequences. First, matching the observed X-ray/TeV lightcurves (as opposed to simply fitting snapshot spectra obtained many days apart) provides a very stringent test of the SC emission model since we have *two* detailed handles on the *single* electron distribution responsible for both emission components. The test can rule out alternate “hadronic” models like that of Dar & Laor (1997), where decaying pions produce an additional, non-Compton  $\gamma$ -ray component. Second, if the SC model works during a large flare (where the emission from a single region may dominate), then we can try to use the observed X-ray spectrum to predict the TeV spectrum. This is key since even for nearby HBLs like Mrk 421/501, the TeV photons propagating towards us can pair produce on the low energy diffuse extragalactic background radiation (DEBRA) and thus be absorbed (Nikishov 1962). If this absorption is present, the usual SC X-ray/TeV spectral modeling of snapshot spectra (e.g., Mastichiadis & Kirk 1997; Pian et al. 1998)

will fail. Note that by using only the relative time behavior of the X-ray and TeV fluxes to test the SC model, we avoid this problem. With an estimate for the intrinsic SC  $\gamma$ -ray spectrum, then, and *only* then, can we attempt to measure and correct for any absorption. This last possibility is particularly exciting since a measurement constrains the density of the target DEBRA photons, which has implications for galaxy evolution and cosmology (e.g., MacMinn & Primack 1996).

Observational advantages aside, objects like Mrk 421 and 501 are still better candidates. They have subluminal accretion disks, implying a weak radiation field outside the jet. For large flares, a simpler and hence more constraining SSC (synchrotron self-Compton) emission model may thus be sufficient. Even if external photons are important, HBLs give tighter constraints because the Compton scatterings responsible for the TeV  $\gamma$ -rays are probably in the Klein-Nishina limit where the exact target photon energies do not matter. Finally, nearby sources that emit to  $\gtrsim 20$  TeV allow us to probe the DEBRA at 10-30  $\mu\text{m}$ , the range most difficult to constrain via other techniques. In sum, simultaneous X-ray and TeV observations of nearby HBLs can tell us much about AGN jet emission mechanisms and the level of the infrared/optical (IR/O) DEBRA – but only if *both* aspects of the problem (the emission and the absorption) are attacked concurrently. In §2 below, we review how  $\gamma$ -ray spectra are modified by absorption and show that its effects may be important even in Mkn 421/501. In §3, we show examples of the rich spectral variability that even simple SSC models can produce as well as useful timing diagnostics to probe it. If an SC model works, we demonstrate how to robustly estimate the shape of the TeV spectrum using X-ray data. We conclude in §4.

## 2. Gamma-Ray Pair Production on Diffuse Background Radiation

The interaction of GeV/TeV radiation with the IR/O DEBRA has received considerable attention, e.g., see Madau & Phinney (1996), MacMinn & Primack (1996), Coppi & Aharonian (1997), Biller et al. (1998), Stanev & Franceschini (1998), and Stecker & DeJager (1998) for some of the recent papers. A detailed discussion of the relevant transfer equations can be found there. In general, to obtain the mean free path for a  $\gamma$ -ray of energy  $E_\gamma$ , one must convolve the DEBRA photon number distribution,  $n(\epsilon)$ , with the pair production cross-section (e.g., see Gould & Schröder 1966). However, this cross-section is peaked and for nearby ( $z \ll 1$ ) HBLs and almost all plausible DEBRA shapes, over half the interactions occur on DEBRA target photons with energies  $\epsilon = 0.5 - 1.5\epsilon_*$ , where  $\epsilon_* = 4m_e^2c^4/E_\gamma \approx 1.04(E_\gamma/1\text{TeV})^{-1}$  eV. To accuracy better than  $\sim 40\%$ , we can thus

approximate the absorption optical depth as

$$\tau_{\gamma\gamma}(E_\gamma) \approx 0.24 \left( \frac{E_\gamma}{1 \text{ TeV}} \right) \left( \frac{u(\epsilon_*)}{10^{-3} \text{ eV cm}^{-3}} \right) \left( \frac{z_s}{0.1} \right) h_{60}^{-1}.$$

Here  $u(\epsilon_*) = \epsilon_*^2 n(\epsilon_*)$  is the typical energy density in a energy band centered on  $\epsilon_*$ ,  $h_{60}$  is the Hubble constant in units of  $60 \text{ km s}^{-1} \text{ Mpc}^{-1}$ , and  $z_s$  is the source redshift. If  $I_0(E_\gamma)$  is the intrinsic source spectrum, the corresponding observed spectrum is then  $I(E_\gamma) = I_0(E_\gamma) \exp(-\tau_{\gamma\gamma})$ . Note that if the DEBRA spectrum near  $\epsilon_*$  can be approximated by a power law,  $n(\epsilon) \propto \epsilon^{-\alpha}$ , then  $\tau_{\gamma\gamma}$  at energies  $E \sim E_\gamma$  goes as  $E^{\alpha-1}$ . Connecting the COBE far IR measurements to the latest UV background estimates, one gets a crude DEBRA spectral index  $\alpha \sim 2$  (e.g., see Dwek et al. 1998 for a good compilation of the latest DEBRA observations and models). To zeroth order, then,  $\tau_{\gamma\gamma} \propto E_\gamma$ , and the observed spectrum should be  $\sim I_0(E_\gamma) \exp(-E_\gamma/E_c)$  where the cutoff energy  $E_c$  is set by  $\tau_{\gamma\gamma}(E_c) = 1$ . Interestingly, this is exactly the type of shape seen in Mrk 501 by Whipple (Samuelson et al. 1998) and especially by HEGRA, which measured the spectrum in the exponential tail up to energies  $\sim 20$  TeV (Aharonian et al. 1999b). Does this mean we are seeing absorption? No. The inset in the upper right corner of Fig. 1 shows a Mrk 501-like SSC spectrum in the TeV energy region. The dotted and dashed curves respectively show the absorbed spectra for an IR/O DEBRA level at the low end of estimates ( $u_l = 2 \times 10^{-4} \text{ eV cm}^{-3} \text{ s}^{-1}$ ) and at the high end ( $u_h = 2 \times 10^{-3} \text{ eV cm}^{-3} \text{ s}^{-1}$ ) assuming a source redshift  $z_s$  and taking  $\alpha = 2$ . The absorbed spectra look just like unabsorbed spectra from blazars with lower cutoffs in their electron energy distributions. To next order, the DEBRA is better described as the sum of two emission components ( starlight from galaxies peaking at  $\sim 1$  eV, and dust re-emission peaking at  $\sim 100 \mu\text{m}$ ). In models, the  $1 - 10 \mu\text{m}$  side of the “valley” between the DEBRA emission peaks is typically a power law with  $\alpha \sim 1$ . At the corresponding  $E_\gamma \sim 1 - 10$  TeV, roughly the energy range of current TeV detectors,  $\tau_{\gamma\gamma}$  is thus almost constant! The shape of the spectrum is unchanged and again we cannot infer absorption. Note that recent results at  $\epsilon_* \sim 3 \mu\text{m}$  (Dwek & Arendt 1998) give a high DEBRA energy density,  $u(3 \mu\text{m}) \sim 2 \times 10^{-3} \text{ eV cm}^{-3} \text{ s}^{-1}$ . Even for Mkn 501 ( $z_s = 0.03$ ),  $\tau_{\gamma\gamma} \approx 0.5$  at  $E_\gamma \sim 3$  TeV, i.e., absorption corrections may be important ( $I_0/I \sim 2$ )! For a  $z_s \sim 0.1$  like that of PKS 2155-304 (a possible TeV source, see Chadwick et al. 1999), they are almost certainly important. The strongest DEBRA constraints may in fact come from energies  $E_\gamma \sim 10 - 30$  TeV, which probe DEBRA energies on the “other” side of the valley ( $\epsilon_* \sim 5 - 60 \mu\text{m}$ ). Here,  $\alpha > 2$  and absorption should grow *super-exponentially* with  $\gamma$ -ray energy. To resolve such sharp absorption cutoffs requires good energy resolution,  $\Delta E/E \lesssim 20\%$ , which appears achievable by Cherenkov arrays operating in stereoscopic mode (Aharonian et al. 1997).

### 3. SC Emission Models and the Intrinsic Gamma-Ray Spectra of Blazars

To test SC models one first requires a theoretically accurate and realistic emission model. Although there are many SC calculations in the literature, we caution that many do not apply to HBLs such as Mrk 421/501 where much of the Compton scattering is probably in the Klein-Nishina regime. The key differences in this regime are that an electron scattering off low energy photons loses essentially *all* its energy to the photon and Compton cooling becomes inefficient compared to synchrotron cooling. This changes, for example, the mapping between the synchrotron and  $\gamma$ -ray emission components. In HBLs, the peaks of the synchrotron and Compton emission components are *not* produced by electrons of the same energy. Also, the Compton ( $\gamma$ -ray) flux at the highest energies will tend to track the X-ray synchrotron flux only *linearly* (e.g., see Ghisellini, Maraschi, & Dondi 1996), instead of quadratically as expected in the Thomson case. Approximations such as using a Klein-Nishina “cutoff” for the Compton cross-section, or solving for the electron energy distribution using a continuous energy loss approximation are dangerous when applied to HBL objects and can easily lead to quantitative errors of factors of several in the spectra predicted for the peaks and tails of the Compton and synchrotron components (e.g., Coppi & Blandford 1990, Coppi 1992).

To illustrate the wide range of time behavior possible in even a simple, one-zone, homogeneous SSC model, we present calculations using the code of Coppi (1992). This code is fully self-consistent and uses no approximations for the emission processes. The calculations in Fig. 1-3 use basic parameters which reasonably describe the time behavior of Mrk 421 (Mastichiadis & Kirk 1997), except we increase the electron cutoff energy by a factor 30 to model Mrk 501 (which has higher energy synchrotron emission, better suited for our purposes). Figure 2 shows the model’s response to three types of variations: (Fig. 2a) the electron injection compactness  $l_e$  ( $= L_e \sigma_T / R m_e c^3$ , where  $R$  and  $L_e$  are respectively the rest frame source radius and electron luminosity) varies randomly by  $\pm 50\%$  every light crossing time ( $R/c$ ) with all other parameters kept fixed, (Fig. 2b)  $l_e$  varies as in Fig. 2a but now the electron cutoff energy also varies with  $l_e$  ( $\gamma_0 \propto l_e$ ), and (Fig. 2c)  $l_e$  varies in Fig. 2a but now the magnetic field varies with  $l_e$  ( $B \propto l_e$ ). Note that for rapid, small variations, the Compton  $\gamma$ -ray flux tracks the synchrotron X-ray flux linearly, i.e., not in the standard quadratic manner. In the Klein-Nishina limit, the main target photons for producing TeV  $\gamma$ -rays are IR/O synchrotron photons. These are produced by low energy electrons with very long cooling times ( $> R/c$ ) that cannot respond quickly to rapid ( $\sim R/c$ ) changes in the electron injection ( $l_e$ ). If one cannot directly observe the IR/O emission (which in real sources may be dominated by emission from other parts of the jet), this means it is *not* obvious what target photon distribution to use when fitting observations. Note that in general, the responses in Fig. 2a-c look quite different, i.e., good timing studies are

a powerful diagnostic. With well-sampled lightcurves, we can make (DEBRA absorption independent!) cross-correlation diagrams such as Fig. 3. At keV energies, in curves (a) and (b) of Fig. 3, we see soft-hard lag behavior (due to the finite electron cooling times) similar to that observed in Takahashi et al. (1996). Such behavior is washed out, though, when the magnetic field changes significantly during a flare (curve c) and the mapping between observed synchrotron photon energy and emitting electron energy is destroyed. At  $\sim 100$  keV, we also clearly see the transition from synchrotron emission to Compton emission: the lag jumps up suddenly because the Compton radiation comes from *lower* energy electrons. The  $\gamma$ -ray to X-ray lag decreases with increasing energy, but does *not* go to zero. In an SSC model, it takes at least  $\sim R/c$  to significantly change the target photon intensity in the source. If the target photons are external and do not vary, no such lag should be seen.

Figure 2 also shows behavior that allows us to make robust predictions for HBL  $\gamma$ -ray spectra. Note the  $\gamma$ -ray hardness ratios in Fig. 2a and 2c fluctuate very little. When the cooling of energetic electrons is dominated by synchrotron radiation, the *only* way to change the shape of the cooled electron distribution is to change the shape of the electron injection function (e.g., as in Fig. 2b). Since the TeV gamma-ray spectrum in this case is essentially the cooled TeV electron distribution, the shape of the  $\gamma$ -ray spectrum is insensitive to most source parameters. In particular, it does not depend strongly on the target photon distribution, as shown in Fig. 1, where a completely different distribution gives the same Compton spectrum (long-dashed curved in the inset). If we can “invert” the observed synchrotron X-ray spectrum to obtain the underlying electron distribution (e.g., as in Fig. 1), we have all we need to predict the shape of the upscattered TeV spectrum. Extrapolating from the spectrum observed at low energies where intergalactic absorption should not be important (e.g., 700 GeV in Fig. 1), we can then predict the unabsorbed flux at TeV energies. Our accuracy is limited by uncertainties in  $B_0$ ,  $\delta$ , and the possible presence of external, low energy IR target photons (with too many such photons, an electron does not lose most of its energy in a typical Compton scattering). However, bad estimates of  $B_0$  and  $\delta$  only cause an overall energy shift of the predicted  $\gamma$ -ray spectrum by a factor  $(\frac{\delta}{B})^{1/2}$  (see Fig. 1), i.e., a fairly weak dependence. Also, the rest frame energy density of external IR photons must exceed the synchrotron photon energy density to cause significant deviations in the predicted spectrum. This is possible, but not likely in HBLs. The inset of Fig. 1 shows the maximum error we could produce by playing with  $\delta$ ,  $B$ , and  $\lambda_s^l$  (which controls the number of low-energy target photons) while requiring the prediction to match the observed 200 – 700 GeV spectrum. This corresponded to about a factor three uncertainty at 10 TeV – not bad considering our minimal assumptions and that typical DEBRA models predict strong absorption at such energies.

#### 4. Conclusions

Mrk 421/501 and similar HBL sources provide ideal laboratories to test in detail the emission models for these objects. If we can show that a simple SC model works during at least the strongest flares, then we can use good broadband X-ray spectra of these sources to infer their intrinsic TeV spectra. Then, and only then, can we look for evidence of  $\gamma$ -ray absorption and attempt to constrain the IR/O DEBRA. (Blazar modelers should not forget that the Compton spectra they are trying to fit could be strongly attenuated!) In any single observation, the absorption might be due both to intrinsic blazar IR/O photons as well as intergalactic ones. While these contributions can be difficult to disentangle, Mrk 421 and 501 conveniently have the same redshift. Thus, we can require that any absorption attributed to intergalactic photons be exactly the same for *all* flares in *both* sources. These two sources alone may give us the first firm handle on DEBRA  $\gamma$ -ray absorption.

#### 5. Acknowledgments

PSC was supported by NASA grant NAG 5-3686 and thanks the Max-Planck-Institut für Kernphysik for its generous hospitality.

#### REFERENCES

- Aharonian F.A. et al, 1997, *Astroparticle Phys.*, vol.6, p,369
- Aharonian F.A., Akerlof C.W. *Ann Rev. Nucl. Part. Sci.* 1997, v. 47, p.273
- Aharonian, F.A. et al. 1999a, *A&A*, 342, 69
- Aharonian, F.A. et al. 1999b, *A&A*, submitted (astro-ph/9903386)
- Biller, S.D. et al 1998, *Phys. Rev. Lett.*, 80, 2992
- Chadwick P.M. et al., 1999, *Astropart. Phys.*, in press
- Coppi, P.S. & Blandford, R.D. 1990, *MNRAS*, 245, 453
- Coppi, P.S. 1992, *MNRAS*, 258, 657
- Coppi, P.S. 1997, in *Relativistic Jets in AGNs, Cracow 1997*, ed. M. Ostrowski, M. Sikora, G. Madejski, & M. Begelman (Cracow: Jagellonian University Press), p. 333 (astro-ph/9903162)

- Coppi, P.S. & Aharonian, F.A. 1997, *ApJ*, 487, 95
- Dar, A. & Laor, A., 1997, *ApJ*, 478, 5
- Dwek, E. et al. 1998, *ApJ*, 508, 106
- Dwek, E. & Arendt, R.G. 1998b, *ApJ*, in press
- Ghisellini, G., Maraschi, & Dondi, L. 1996, *A&AS*, 120, 503
- Gould, R.J. & Schréder, G. 1966, *Phys. Rev. Lett.*, 16, 252
- MacMinn, D. & Primack, J.R. 1995, *Space Sci. Revs.*, 75, 413.
- Madau, P. & Phinney, E. 1996, *ApJ*, **456**, 124
- Mastichiadis, A. & Kirk, J., 1997, *A&A*, 320, 19
- Nikishov, A.I. 1962, *Sov. Phys. JETP*, 14, 393
- Pian, E. et al. 1998, *ApJ*, 492, 17
- Samuelson, F.W. et al. 1998, *ApJ*, 501, 17
- Sikora, M. 1997, in *Proceedings of the Fourth Compton Symposium*, ed. C.D. Dermer, M.S. Strickman, & J.D. Kurfess, *AIP Conference Proceedings* 410, p. 494
- Stanev, T. & Franceschini, A. 1998, *ApJ*, 492, 219
- Stecker, F.W. & DeJager, O.C. 1998, *A&A*, 334, L85
- Takahashi, T. et al. 1996, *ApJ*, 470, 89
- Ulrich, M.H., Maraschi, L., & Urry, *ARA&A*, 35, 445



Fig. 1.— The SSC spectrum (*heavy solid lines*) produced by a spherical source which has rest frame radius  $R = 4.7 \times 10^{16}$  cm, is observed with Doppler boost factor  $\delta = 15$ , and has a tangled magnetic field  $B_0 = 0.07$  Gauss. Electrons enter with an initial (injection) energy spectrum  $d\dot{N}_{inject}(\gamma)/d\gamma \propto (\gamma)^{-s} \exp(-\gamma/\gamma_0)$  down to  $\gamma_{min} = 1.3$ , where  $\gamma$  is the rest frame electron Lorentz factor,  $s = 1.7$ , and  $\gamma_0 = 7 \times 10^6$ . They escape on a rest frame timescale  $t_{esc} = 3.3R/c$ . The spectrum shown is *not* a steady-state, equilibrium spectrum, but rather the integrated flux (from  $t = 0$  to  $50R\delta^{-1}/c$ ) of the time-varying model in Fig. 2a. The *dot-dashed* curve is the synchrotron emission from an electron distribution reconstructed from the 0.1-300 keV X-ray spectrum. (The distribution is obtained by using a delta function emission approximation to initially “invert” the X-ray spectrum and then iterating using the exact synchrotron emission spectrum.) The *dotted* and *dashed* curves in the main figure give the Compton  $\gamma$ -ray spectra predicted from the electron distributions reconstructed assuming two extreme sets of model parameters. The target photon distribution used was not the synchrotron spectrum, but a power law  $n(\lambda) \propto \lambda^2$  extending (in the source frame) from 0.1 to  $\lambda_s^l$  microns. The inset in the upper right corner of the figure shows a blowup of the spectrum in the TeV energy region. The *heavy dot-dashed* and *heavy long-dashed* curves show the predicted gamma-ray spectra for two more realistic sets of parameters. The *dotted* and *dashed* curves give the spectra obtained from a source described by the solid heavy curve after  $\gamma$ -ray absorption by IR/O DEBRAs with energy densities  $u_l$  and  $u_h$ , respectively (see text).

Fig. 2.— The SSC response to variations in electron injection and magnetic field strength (see text). The top of each panel shows the hardness ratios between various (observed) energy bands as a function of observer time. The bottom shows the photon number flux escaping in several (observed) energy bands. The *heavy solid* curve is the total electron injection luminosity ( $l_e(t)$ ) as a function of time (see text) and is the same for all three panels. At  $t = 0$ , the source is assumed to be empty and electron injection is turned on impulsively. The initial value for the total electron compactness (injection luminosity) is  $l_e = 2.4 \times 10^{-4}$ . The flux levels shown are normalized to be the same at  $t \approx 10R\delta^{-1}/c$ . The hardness ratio normalizations have also been adjusted for clarity. Note the flux and hardness ratio axes are logarithmic. The electron escape time is  $3.3R/c$  for the top and bottom panels, and  $333R/c$  for the middle panel.

Fig. 3.— The relative lag/lead of the flux at an observed energy,  $E_{obs}$ , versus the observed flux at 0.3 keV. Here,  $\delta_{15} = \delta/15$  and  $R_{16} = R/10^{16}$  cm where  $\delta$  and  $R$  are respectively the source Doppler factor and radius. The curves labeled (a), (b), (c) are computed by running a cross-correlation analysis on the lightcurves shown in Fig 2a, b, and c, respectively, and plotting the lag/lead times at which the cross-correlation functions peak. (The cross-correlation functions are relatively narrow for the lightcurves of Fig. 2.)

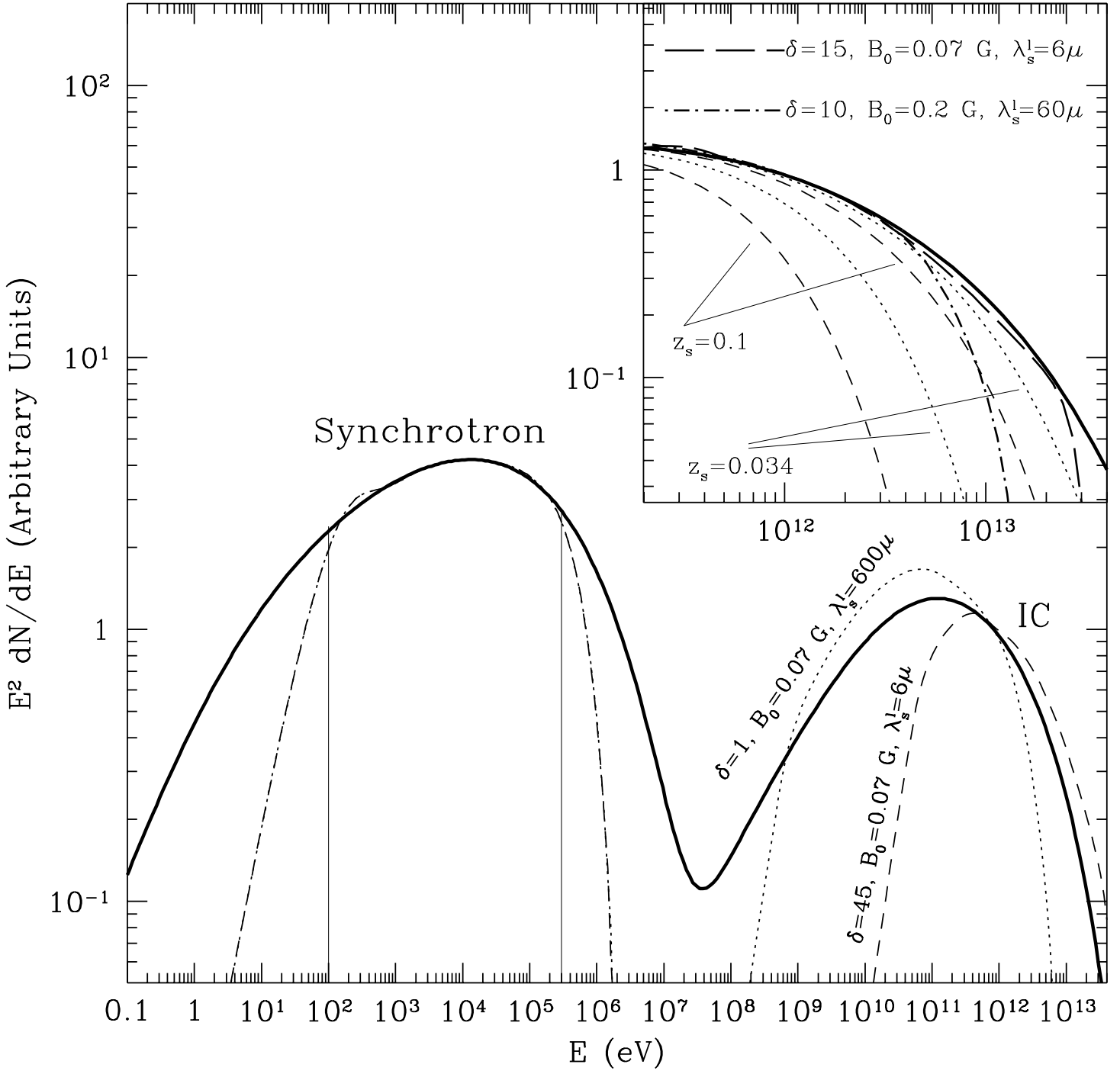


Figure 1

Figure 2

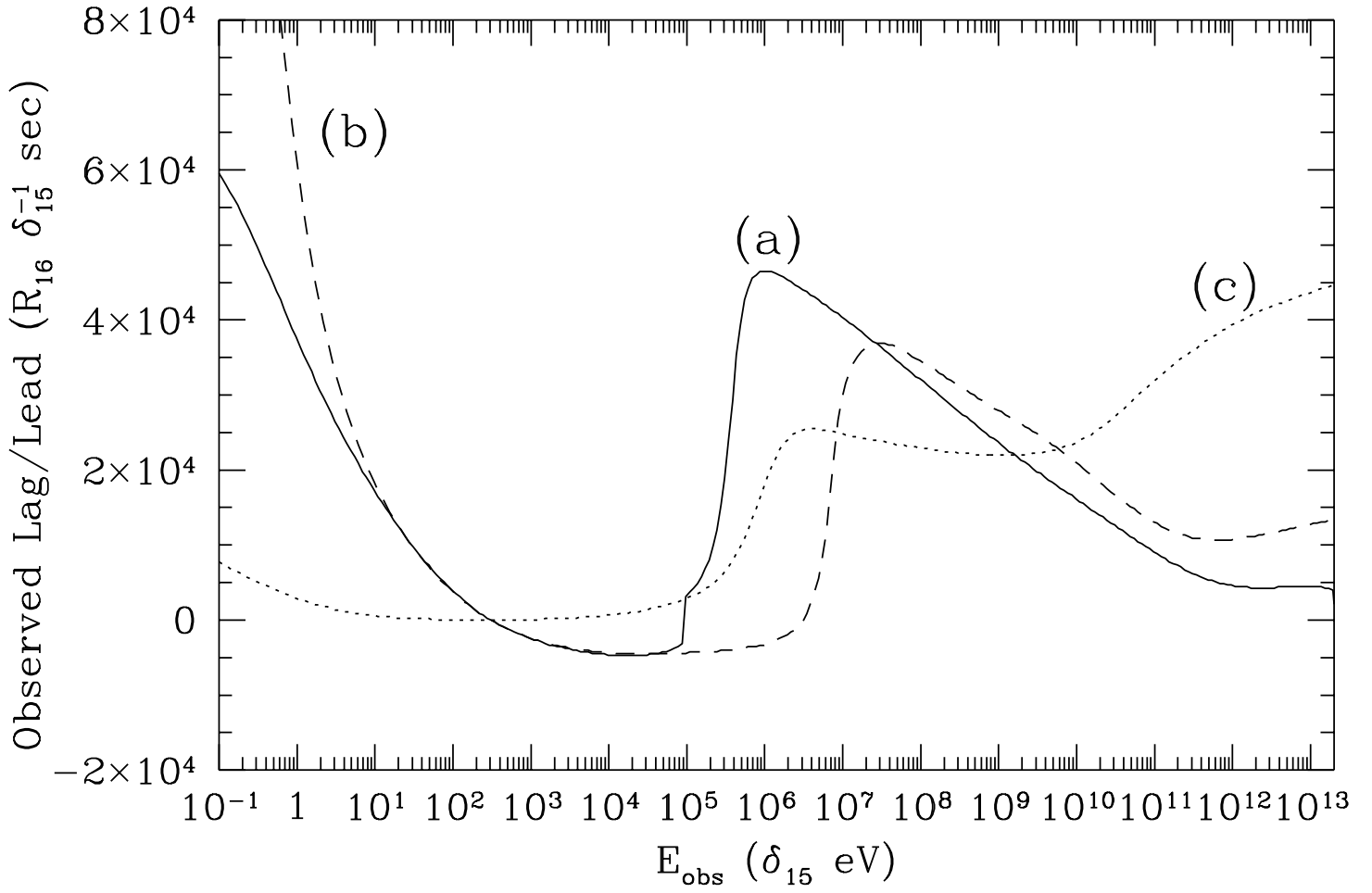


Figure 3

